Numerical Prediction of the Unsteady Flow and Radiated Noise from a 3D Lifting Airfoil

E. Manoha, S. Redonnet, C. Delahay
P. Sagaut, I. Mary
Department of Computational Fluid Dynamics
and Aeroacoustics
ONERA, BP 72, 92322 Châtillon, France
eric.manoha@onera.fr

S. Ben Khelil, P. Guillen
Department of Applied Aerodynamics
ONERA, BP 72, 92322 Châtillon, France
eric.manoha@onera.fr

ABSTRACT

The numerical prediction of the aerodynamic noise radiated by an isolated airfoil is performed using a Computational AeroAcoustics (CAA) method. This hybrid method combines (i) a simulation of the nearfield unsteady flow and (ii) an acoustic method to estimate the noise radiated in the far field. This process is applied to a symmetrical NACA0012 airfoil with a constant section and a blunted trailing edge (TE), at a Mach number of 0.205 and an angle-of-attack of 5°. The Reynolds number based on the airfoil chord is 2.86 millions. The computational domain has a spanwise extent representing 3.3 % of the chord.

The nearfield unsteady flow around the airfoil is computed via a compressible three-dimensional Large Eddy Simulation (LES). This flow exhibits a superimposed pressure fluctuation field which presents the qualitative and quantitative features of the TE noise generated by the acoustic scattering of (i) the turbulent boundary layers convected on both airfoil sides (broad-band noise) and (ii) the alternated vortex shedding generated by the TE bluntness (narrow band component). Due to the strong stretching of the LES computational grid, which acts as an acoustic low-pass frequency filter, this acoustic field cannot radiate farther than a half-chord from the body.

Consequently, the LES must be relayed by an acoustic propagation method to correctly simulate the farfield noise. The most readily available methods are integral techniques which only need data on a control surface or in a control volume. A former estimation is performed via the Kirchhoff integration of pressure data on a control surface enclosing the airfoil and its wake. The position of this surface is subjected to a careful parametric study. Since very large spanwise integral lengh scales are observed on this surface, the acoustic field is assumed two-dimensional there, leading to interesting qualitative results but overestimated noise levels. On the other hand, wall pressure spanwise integral lengh scales reasonably match experimental values, suggesting to use the Ffowcs Williams-Hawkings integration of wall pressure data. This method provides farfield noise levels which agrees well with experimental data.

Both methods assume that the mean flow is uniform outside the control surface, which slightly distorts the solution since the actual flow is non-homogeneous. In order to avoid such distorsion, one can resort to a numerical method based on discretized linearized Euler equations (LEE) in which the total field is splitted into a mean flow and a pertubation field. The E3P code (Propagation of small perturbations using Euler equations) is currently developed for that purpose. The present paper shows its application to several complex acoustic scattering problems, then it shows how this code could be coupled to LES calculation on a two-dimensional interface.

NOTATIONS

a_0 : sound celerity in the fluid at rest,
Δ : characteristic length scale,
$\overline{F_j}$: inviscid fluxes,
$\overline{F_j^v}$: viscous fluxes,
f_{θ_0} : selective function $f_{\theta_0}(\theta)$,
Φ : wavenumber-frequency spectrum $\Phi(k,\omega)$,
H : trailing edge thickness,
k : wavenumber,
κ : local instantaneous fluid thermal conductivity,
κ_0 : thermal conductivity of the fluid at rest,
K_c : small scale kinetic energy,
λ_a : Acoustic wavelength $\lambda_a = \omega/c_0$,
M_0 : flow Mach number $M_0 = U_0/a_0$, $M_0^2 = U_0^2/\gamma R T_0$,
μ : local instantaneous dynamic fluid viscosity,
μ_0 : dynamic viscosity of the fluid at rest,
μ_t : turbulent dynamic viscosity,
$\overline{n}$: unit vector normal to S, oriented towards outside,
ω : frequency,
p : local instantaneous pressure in the flow,
p_0 : pressure of the fluid at rest,
p' : pressure fluctuation, identified with acoustic pressure in the far field $p' = p - p_0$,
$\overline{Q_c}$: conservative flow variable,
ρ : local instantaneous density in the flow,
ρ_0 : density of the fluid at rest,
ρ' : density fluctuation in the flow $\rho' = \rho - \rho_0$,
P_r : Prandtl number $P_r = \mu_0 C_p / \kappa_0$
R_e : Reynolds number $R_e = \rho_0 U_0 C / \mu_0$,
S_{ij} : filtered shear stress tensor $S_{ij}(\tilde{u})$,
S : Kirchhoff integration surface,
TE : trailing edge,

Paper presented at the RTO AVT Symposium on "Ageing Mechanisms and Control: Part A – Developments in Computational Aero- and Hydro-Acoustics", held in Manchester, UK, 8-11 October 2001, and published in RTO-MP-079(I).

TBL : turbulent boundary layer,
$\vec{X}$: observer location in the airfoil framework,
$\vec{Y}$: source location in the airfoil framework,
t : reception time,
τ : emission time,
T : local instantaneous fluid temperature,
T_0 : temperature of the fluid at rest,
$\vec{u}$: local instantaneous fluid velocity,
U_0 : upstream flow velocity,
U_e : local mean flow velocity outside the boundary layer.

INTRODUCTION

The aerodynamic noise generated by the high lift devices - HLD, slats and flaps - of large airliners is an important contributor to the total radiated airframe noise, especially in approach configuration. It is widely admitted that this noise source will have to be reduced for the next generation of aircraft to meet the incoming strengthened noise regulations in the vicinity of airports. This goal will be reached by the design of new HLD concepts incorporating specific noise reduction devices. Although experiment will still play an important role in the design of such devices, it is thought that significant results will be obtained, with lower costs and shorter delays, from the numerical simulation, particularly considering the spectacular continuing progress of Computational AeroAcoustics (CAA) applications.

At the present time, the problem of the numerical simulation of HLD noise is still beyond the capabilities of complete Direct Numerical Simulation (DNS). It is most likely that, in the next future, only hybrid methods, in which the nearfield turbulent flow and the farfield noise are computed separately, will be able to solve complex aeroacoustic problems involving HLD.

Several Computational Fluid Dynamics (CFD) techniques are used in CAA hybrid methods. The less computationally expensive methods are based on steady Reynolds-Averaged Navier-Stokes (RANS) computations, in conjonction with stochastic models of the wavenumber-frequency spectrum of the turbulence [1]. RANS methods are also used to compute unsteady flows around airfoils for aeroacoustic predictions [2,3], but Large Eddy Simulation (LES) is often considered as one of the most promising method in the context of CAA applied to HLD noise [4,5,6].

On the other hand, a large panel of acoustic techniques, with various complexity and capabilities, can be used for the prediction of farfield noise. The most practical formulations belong to the family of integral methods such as (i) acoustic analogies, including Lighthill's analogy [5,7] and the Ffowcs Williams-Hawkings (FW-H) equation [2,3,8], (ii) the Boundary Element Method (BEM) [9] and (iii) the Kirchhoff integration method.

Most integral methods assume that, beyond a given distance from the noise sources and body surfaces, the sound propagates in a medium at rest, or moving with uniform velocity. This assumption may become a strong limitation, especially when the radiated noise results from a surface integration on a control surface which is located near solid walls where velocity gradients are significant. In that case, only the discretized LEE, the equations governing the acoustic propagation, may account for the propagation in non-homogeneous flows. Although Euler equations have been widely used in CFD applications in the past, this know-how is of little help for acoustic simulation, since higher order schemes are needed to ensure numerical accuracy and low dispersion of acoustic waves [10]. At the present time hybrid CAA methods combining unsteady CFD and discretized LEE have only been applied to free field flows like jets and mixing layers, for which cartesian grids make computations particularly convenient. Their application to realistic geometries including airfoils needs curvilinear grids [11,12] on which the use of high order finite difference schemes is not straightforward.

First CAA studies at ONERA focused on trailing edge (TE) noise of isolated airfoils, a basic aeroacoustic mechanism which is present in complex HLD geometries. In an former study [5], only the uncompressible unsteady flow at the vicinity of the TE was simulated via LES, which was valid since aeroacoustic sources of such an airfoil are known to be concentrated in this region. For this purpose, the TE was modelled by a thick flat plate with an imposed mean velocity profile of a realistic boundary layer on each side. This simplification was also governed by the capabilities of PEGASE, the used LES code which only handled cartesian meshes. Then the radiated noise was obtained using the formulation Ffowcs Williams-Hall [13] based on Lighthill's acoustic analogy and the acoustic Green's function of an infinite half-plane (an approach that has been recently followed by Wang [6]). Despite encouraging results, this exploratory study presented two major weaknesses since (i) the exact airfoil shape was not correctly taken into account in the mechanism of acoustic diffraction of quadrupolar sources and, (ii) the flow simulation did not comprise the whole airfoil.

In a more recent study [9], point (i) was addressed by the use of an innovative acoustic method, also based on Lighthill's acoustic analogy, but associated to a Boundary Element Method to compute the exact acoustic Green's function of the studied airfoil. The method was restricted to cylindrical infinite surfaces with constant sections, for which the determination of the 3D acoustic Green's function is narrowed to a much simpler 2D problem and to acoustic radiation in far field. The application of this method to more realistic airfoil shapes (a NACA 0012 symmetrical profile and a high lift wing section with slat and flap), but with non-realistic unsteady flows, showed that, as long as the unsteady three-dimensional flow is known in the vicinity of a scattering surface of any shape, the resulting radiated noise can be predicted. Consequently, this method is particularly attractive when the turbulent flow is computed, for example by using LES, in a domain which covers only a small fraction of the whole rigid surface.

The present paper addresses point (ii), the objective being to perform an acoustic prediction based on the LES of the unsteady flow around a 3D lifting airfoil with a blunted TE.

The paper is organized as follows. The first part of the paper is devoted to the unsteady flow simulation via LES. The theoretical background of LES and its implementation in an in-house industrial CFD software are described. Then the airfoil geometry and the computational grid are presented, as well as the numerical procedure and storage method. A few basic aerodynamic results are given at the end of this part.

In the second part, the pressure field computed via LES near the airfoil is analyzed in details. It exhibits the qualitative and quantitative features of an acoustic field noise, generated by the acoustic scattering at the airfoil TE of (i) the turbulent boundary layers convected on both sides (broad-band noise) and (ii) the alternated vortex shedding generated by the TE bluntness (narrow band component). It is shown that, due to the strong

stretching of the LES computational grid, which acts as an acoustic low-pass frequency filter, this acoustic field cannot radiate farther than a half-chord from the body. Consequently, the LES must be relayed by an acoustic propagation method to correctly simulate the farfield noise. The most readily available methods are integral techniques which only need data on a control surface or in a control volume.

The third part of the paper presents a noise estimation performed via the Kirchhoff integration of pressure data on a control surface enclosing the airfoil and its wake. The position of this surface is subjected to a careful parametric study. Since very large spanwise integral lengh scales are found on this surface, the acoustic field is assumed two-dimensional there, leading to interesting qualitative results but overestimated farfield noise levels.

On the other hand, wall pressure spanwise integral lengh scales reasonably match experimental values, which suggested to use a Ffowcs Williams-Hawkings integration of wall pressure data. This application is presented in the fourth part of the paper. This method provides farfield noise levels which agrees well with experimental data.

However, both integral methods assume that the mean flow is uniform outside the control surface, which may distort the solution if the actual flow is non-homogeneous. In order to avoid such distorsion, one has to resort to a method based on discretized LEE in which the total field is splitted into a mean flow and a pertubation field. The E3P code (Propagation of small perturbations using Euler equations) is currently developed for that purpose. The fifth part of the paper shows its application to several complex acoustic scattering problems, then it shows how this code could be coupled to LES calculation on a two-dimensional interface.

LARGE EDDY SIMULATION

Code implementation

The LES method described below has been implemented in the FLU3M solver, an industrial CFD software which has been developed at ONERA for several years. This solver is based on the discretization of the compressible Navier-Stokes equations on multi-block structured meshes by a finite volume technique. A second order accurate implicit temporal integration is achieved thanks to an approximate Newton method. General informations about this solver are available in refs. [13,14].

Governing equations

Filtered Navier-Stokes equations

A dimensionless form of the Navier-Stokes equations is retained, which means that, in equations (1) to (8), the local instantaneous velocity $\overline{u}$, temperature T, density ρ, abscissa $\overline{x}$, dynamic viscosity μ and thermal conductivity κ are normalised respectively by U_0, T_0, ρ_0, C, μ_0 and κ_0.

The three-dimensional unsteady filtered Navier-Stokes equations are used for a viscous compressible Newtonian fluid. Any flow variable ϕ can be written as $\phi = \overline{\phi} + \phi'$, where $\overline{\phi}$ represents the large scale part of the variable and ϕ' its small scale part. The filtering operator, classicaly defined as a convolution product on the computational domain [16], is assumed to commute with time and spatial derivatives. Moreover it is convenient for the clarity of the equations to introduce the Favre filtering $\tilde{\phi} = \overline{\rho\phi}/\overline{\rho}$. In conservative form, the filtered Navier-Stokes equations can be expressed in three-dimensional Cartesian coordinates (x_1, x_2, x_3) as :

$$\frac{\partial \overline{Q_c}}{\partial t} + \frac{\partial \overline{F_j}}{\partial x_j} - \frac{1}{R_e}\frac{\partial \overline{F}_j^{\,v}}{\partial x_j} = 0 \qquad (1)$$

where $\overline{Q_c}$, $\overline{F_j}$ and (assuming some approximations [17] and using Boussinesq eddy viscosity hypothesis) $\overline{F}_j^{\,v}$ are defined by :

$$\overline{Q_c} = \begin{pmatrix} \overline{\rho} \\ \overline{\rho}\tilde{u}_1 \\ \overline{\rho}\tilde{u}_2 \\ \overline{\rho}\tilde{u}_3 \\ \overline{\rho E} \end{pmatrix} \quad \overline{F_j} = \begin{pmatrix} \overline{\rho}\tilde{u}_j \\ \overline{\rho}\tilde{u}_1\tilde{u}_j + \delta_{1j}\overline{p} \\ \overline{\rho}\tilde{u}_2\tilde{u}_j + \delta_{2j}\overline{p} \\ \overline{\rho}\tilde{u}_3\tilde{u}_j + \delta_{3j}\overline{p} \\ (\overline{\rho E} + \overline{p})\tilde{u}_j \end{pmatrix} \quad \overline{F}_j^{\,v} = \begin{pmatrix} 0 \\ \overline{\sigma}_{1j} \\ \overline{\sigma}_{2j} \\ \overline{\sigma}_{3j} \\ \overline{\sigma}_{kj}\tilde{u}_k + \overline{q}_j \end{pmatrix} \qquad (2)$$

where $$\overline{\rho E} = \frac{\overline{p}}{\gamma - 1} + \frac{1}{2}\overline{\rho}\tilde{u}_j\tilde{u}_j \qquad (3)$$

$$\overline{\sigma}_{ij} = \left(\mu(\tilde{T}) + \mu_t\right)\left(\frac{\partial \tilde{u}_i}{\partial x_j} + \frac{\partial \tilde{u}_j}{\partial x_i} - \frac{2}{3}\delta_{ij}\frac{\partial \tilde{u}_k}{\partial x_k}\right) \qquad (4)$$

$$\overline{q}_j = \frac{\left(\mu(\tilde{T}) + \mu_t\right)}{P_r}\frac{\partial \tilde{T}}{\partial x_j} \qquad (5)$$

where the eddy viscosity μ_t must be expressed by a subgrid scale model. These equations are supplemented with the filtered equation of state :

$$\overline{p} = \frac{\overline{\rho}\tilde{T}}{\gamma M_0^2} \qquad (6)$$

Subgrid scale modelling

Selective mixed scale model

The selective mixed scale model, developed by Sagaut and Lenormand, has been retained, because it realizes a good compromise between accuracy, stability and computational cost [17,18]. More particularly, the use of a selective function allows to handle transitional flows [19], which is one of the keypoint of the present application.

The eddy viscosity is given by the non-linear combination :

$$\mu_t = \overline{\rho} f_{\theta_0}(\theta) C_m \Delta \sqrt{0.5 S_{ij}(\tilde{u}) S_{ij}(\tilde{u})}\sqrt{K_c} \qquad (7)$$

of the filtered shear stress tensor $S_{ij}(\tilde{u})$, a characteristic length scale Δ (given by the cell volume of the mesh), the small scale kinetic energy $K_c = \sqrt{0.5(\tilde{u}_i')(\tilde{u}_i')}$, a constant parameter C_m = 0.06 (derived in reference [16]) and the selective function :

$$f_{\theta_0}(\theta) = \begin{cases} 1 & \text{if } \theta > \theta_0 = 10° \\ \tan^4(\theta/2) \big/ \tan^4(\theta_0/2) & \text{otherwise} \end{cases} \qquad (8)$$

where θ is the angle between instantaneous and filtered vorticity. The test field $(\tilde{u}_i)'$ is extracted from the resolved field $(\tilde{u}_i)' = \tilde{u}_i - \overline{\tilde{u}_i}$, employing an averaging test filter denoted by : $\overline{\tilde{u}_i} = 0.25\tilde{u}_{i-1} + 0.5\tilde{u}_i + 0.25\tilde{u}_{i+1}$.

Numerical method

The Navier-Stokes equations are discretized using a cell-centered finite volume technique and structured multi-block meshes. The viscous fluxes are discretized by a second-order accurate centered scheme. For efficiency reason, an implicit time integration is employed to deal with the very small grid size encountered near the wall. Indeed the large disparity between the acoustic wave speed and the advection velocity at low Mach number renders explicit time integration unefficient. This is due to the fact that numerical stability considerations impose small time steps on the acoustic waves, while the physics is mainly driven by the solenoidal part of the flow, whose time scale, being associated to advection, is larger. Then a three-level backward differentiation formula is used to approximate the temporal derivative of $\overline{Q}_c$ leading to second-order accuracy. An approximate Newton method is employed to solve the non-linear problem. At each iteration of this inner process, the inversion of the linear system relies on Lower-Upper Symmetric Gauss-Seidel (LU-SGS) implicit method, originally proposed in reference [20]. More details about these numerical points are available in references [21,22].

Usually LES requires high-order centered scheme for the Euler fluxes discretization (with spectral-like resolution) in order to minimize dispersive and dissipative numerical errors. However such schemes cannot be applied easily in complex geometry. Indeed, most of aerodynamic codes able to deal with such a geometry are based on finite-volume technique in order to handle degenerated cell. Thus getting high-order method becomes very time consuming due to high-order quadrature needed to compute the fluxes along the cell boundaries. As several works (see [23] for instance) have shown that LES can be carried out with low-order centered scheme in case of sufficient mesh resolution, only second-order accurate scheme is employed in this study. But a special effort has been carried out to minimize the intrinsic dissipation of the scheme.

Thus the second order accurate hybrid upwind/centered discretisation, developped in [21], has been used in this study to achieve a good compromise between robustness and accuracy. The key point of the scheme is the use of a sensor, which allows to introduce locally some numerical dissipation when a numerical wiggle is detected on one of the primitive variables. Therefore, the effect of the SGS model is not affected by the numerical dissipation as long as odd-even decoupling is not detected in the flow solution.

Geometry, computational grid and numerical procedure

A two-dimensional (constant section in the spanwise direction) NACA 0012 airfoil with a $C = 0.6096$ m chord and a blunted TE of thickness $H = 2.5$ mm (0,4 % of the chord) has been retained for this study, with reference to the airfoil noise experiment conducted at NASA in 1980 by Brooks and Hodgson [24]. In this experiment, the airfoil had a span $S = 0.46$ m (or 75 % of the chord), whereas in the present simulation, the LES computational domain has a spanwise extent representing only 3.3 % of the chord.

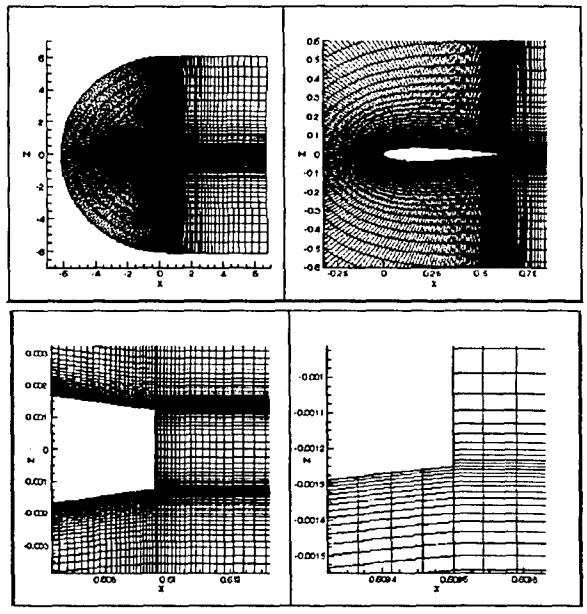

Figure 1 : Computational grid.

The upstream flow velocity is 69.45 m/s (maximal velocity in [24]), the Mach number is 0.205 and the Reynolds number based on upstream velocity and chord is 2.86 millions. The airfoil angle-of-attack with respect to the flow direction is 5°.

The 3D curvilinear computational grid is obtained by replication in the spanwise direction (y) of a 2D curvilinear structured grid made of two domains. Domain #1 is located upstream the TE (C-shape), with 309 points along the airfoil body and 97 points in the radial direction. Domain #2 is located downstream the TE, with 227 points in the (z) direction (including 35 points on the TE bluntness) and 103 points in the (x) direction. In order to minimize the influence of boundary conditions, a large computational domain is used. As shown in Figure 1, this 2D grid extents nearly 10 chords above and below the profil, as well as upstream and downstream. Regions in the vicinity of solid walls are highly refined. The whole mesh is made of 1.76 million points.

The horizontal plane $z = 0$ is a plane of symmetry. In any (x, z) plane, the smallest cells are located at the TE corners, with dimensions (in wall units) $\Delta z^+ = 1.5$ in the direction normal to the wall and $\Delta x^+ = 15$ along the chord. From the corners, the grid is streched in the streamwise direction (x) with a stretching coefficient equal to 1.06 (upstream) and 1.09 (downstream). In the (z) direction, the stretching coefficients are equal to 1.23 towards the $z = 0$ plane and 1.12 towards the grid periphery.

This 2D grid is replicated 32 times in the spanwise direction (y), with a constant step $\Delta y = 10^{-1}C$.

The mesh resolution is close to that of Weber and Ducros [22] who have shown that such resolution is sufficient to obtain reasonable results for such flows.

A no-slip condition is applied at the airfoil surface and a periodic conditon is imposed in the spanwise direction. Non-reflecting characteristic boundary conditions are applied for the far field. Moreover, a steady RANS computation using Baldwin-Lomax models provides an initial flow solution. In order to ensure the time-accuracy of the results, the physical time step is taken equal to 0.5 µs, meaning a sampling frequency of 2 MHz. An initial phase of 100,000 time steps was achieved, then the useful computation was performed over 130,000 time

steps with a total duration of 65 ms, representing the convection of the flow over 7.5airfoil chords. The requirements of acoustic computations led to a storage of one time sample every 100, meaning a storage sampling of 20 kHz, with a useful frequency band of 10 kHz. The total computation cost was 360 CPU hours on a NEC-SX5 computer.

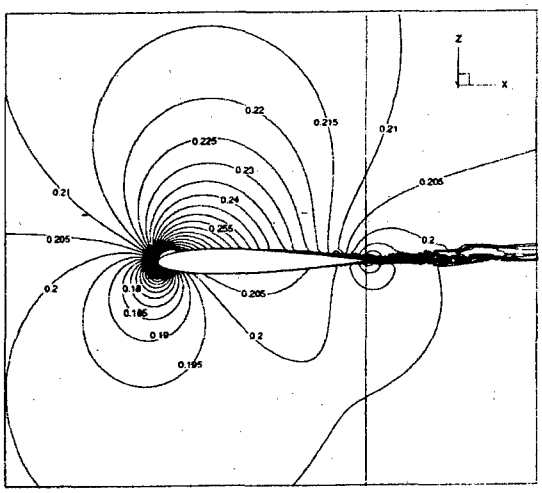

Figure 2 : Contours of instantaneous Mach number isovalues.

Aerodynamic results

Figure 2 displays contours of instantaneous Mach number isovalues, showing the development of the TBLs and the wake. The transition between laminar and turbulent flows occurs at $x/C = 0.15$ on the succion side and at $x/C = 0.9$ on the pressure side. Mean velocity profiles near the TE were obtained by time-averaging instantaneous data. The integration of these velocity profiles provided TBL momentum thicknesses of $\delta_1 \approx 0.8$ mm on the pressure side and $\delta_1 \approx 1.5$ mm on the succion side. Brooks and Hodgson's [24] measurement on a similar airfoil was slightly higher ($\delta_1 \approx 3.9$ mm), which could be explained by the roughness strips of carbon random they used to artificially trip the boundary layer at x/C = 0.15.

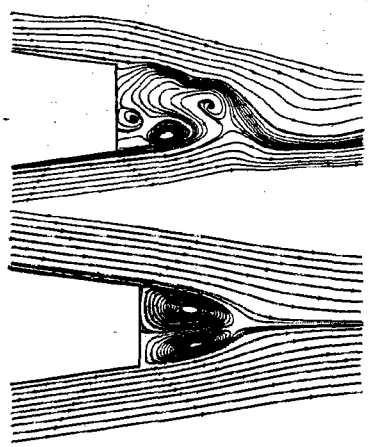

Figure 3 : Flow streamlines at the trailing edge, instantaneous (above) and time-averaged (below).

It is thougth that the excessive slenderness of the computed TBL may be also explained by an unsufficient grid refinement in the chord direction x near the walls in the transition region. However, it will be shown in the next part that the computed flow presents general qualitative and quantitative features which makes it suitable for aeroacoustic applications.

Figure 3 shows details of the instantaneous (above) and time-averaged (below) flow streamlines around the blunted trailing edge. Time-averaged results have been favourably compared with the results of the mean flow computed separately using a RANS code.

UNSTEADY PRESSURE FIELD ANALYSIS

Surface pressure fluctuations

Time histories

Figure 4 (above) shows time histories of the wall pressure fluctuations near the TE at symmetrical points located on the pressure and succion sides. This plot exhibits a time period of 2 ms, meaning a dominant mechanism at a frequency near 5 kHz, and a clear phase opposition between both sides. This opposition is confirmed by the cross-spectrum phase between boths signals shown on Figure 4 (bottom). These features are typical of a mechanism of alternated vortex shedding at the TE.

Power spectral densities

Figure 5 shows the evolution along the chord (from the leading edge up to the TE) of the wall pressure power spectral density (0-10 kHz) on the succion side (above) and the pressure side (below). Spectra are characterized, on both airfoil sides, by a narrowband component emerging out of a wideband continuum.

Located near 4.7 kHz, the narrowband bump is due to the vortex shedding mechanism. It is perceived on the whole chord length with identical levels on both airfoil sides. It will be shown later that this component corresponds to acoustic waves generated at the TE and propagating in the upstream direction.

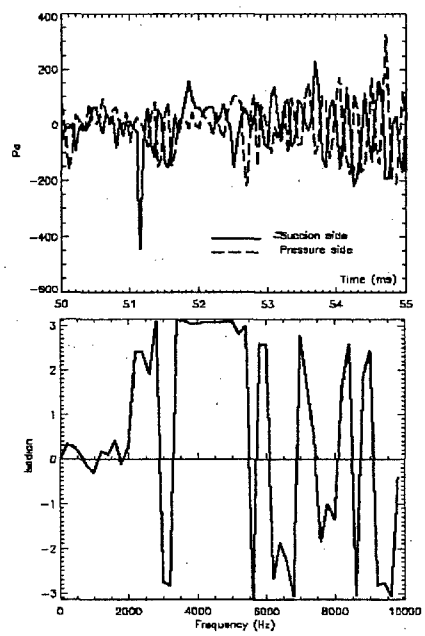

Figure 4 : Wall pressure fluctuations on pressure and succion sides near the TE. Above : time histories. Below : cross-spectrum phase.

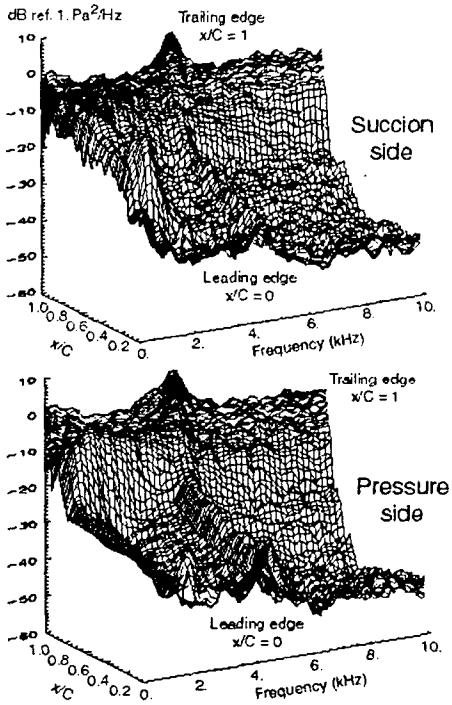

Figure 5 : Evolution of the wall pressure PSD along the chord.

The wideband continuum is generated by the convected turbulent boundary layers. Since the airfoil has a positive 5° angle-of-attack, the laminar-to-turbulent transition occurs at 15% of the chord on the succion side, and at 90% of the chord on the pressure side. From this transition point towards the TE, the boundary layer thickness grows, enriching spectra with higher frequency components. Notice that, on both airfoil sides, the vortex shedding component emerges from the continuum near the TE ($x/C > 0.98$), then is masked by the nearfield boundary layer, and finally emerges again at $x/C < 0.85$.

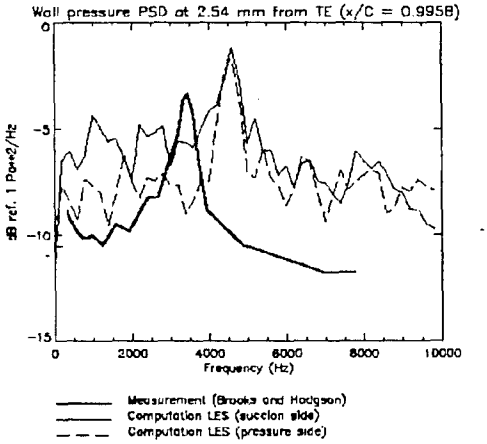

Figure 6 : Wall pressure PSD near the TE. Comparison of simulation (both airfoil sides) and experiment [24].

<u>*Comparison to experimental data*</u>

In their airfoil noise experiment (performed with same velocity, tripped TBL, but zero incidence) [24], Brooks and Hodgson measured surface pressure with arrays of pinhole sensors of diameter 0.34 mm. The closest distance between sensors and the TE was at 2.54 mm. Figure 6 compares the spectrum measured by this sensor with simulated data computed data at the same position ($x/C = 0.9958$). The comparison is qualitatively satisfying : same narrowband component emerging by ≈7 dB from a wideband continuum. However, the quantitative comparison shows that predicted levels are overestimated by nearly 3 dB, and that the predicted vortex shedding frequency (4.7 kHz) is also overestimated (3.5 kHz in the experiment). Since this frequency is governed by a Strouhal number based on the wake thickness (sum of the TE thickness and TBL displacement thicknesses), this overestimation may be partly explained by the excessive slenderness of the computed turbulent boundary layer (TBL) with respect to the experimental one. However this cannot be solely explained by the absence of transition triggering in the simulation.

<u>*Wavenumber-frequency spectra*</u>

The spectral densities presented above are single-point data which do not provide any information on the propagative features of the wall pressure field. This information can be revealed by processing a discretized space-time Fourier transform of any function $p(x,t)$, providing the so-called wavenumber-frequency spectrum $\Phi(k,\omega)$. For example, a mono-dimensional wave with frequency ω_0 and velocity V_0 propagating in the x direction, say $p(x,t) = e^{i\omega_0(t - x/V_0)}$, will appear in the (k,ω) domain as a Delta-function centered at $k = \omega_0/V_0$ and $\omega = \omega_0$. With the same process, a white noise propagating at celerity c_0 in the x direction will appear as a ridge along the $k = \omega/a_0$ line, or along the $k = -\omega/a_0$ line if the sound travels in the opposite (*-x*) direction.

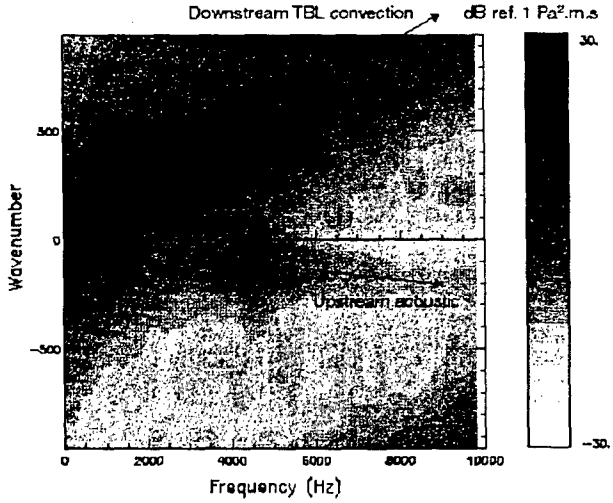

Figure 7 : Wavenumber-frequency spectrum of wall presssure fluctuations on the airfoil succion side at x/C = 0.9.

Figure 7 presents the results of this process applied to the wall pressure field computed via LES on the airfoil pressure side near the TE at $x/C = 0.9$. The wavenumber domain extent $[-\pi/\Delta x, \pi/\Delta x]$ depends on the local space sampling Δx of the pressure field, or the size of the grid cells. A wideband "convective ridge" can be observed along the $k = \omega/U_c$ line, generated by the convection, in the flow direction, of eddies inside the TBL at an average velocity U_c slightly inferior to the local mean flow velocity U_e. Another wideband component can

be observed along the $k = -\omega/(a_0 - U_e)$ corresponding to an acoustic propagation in the direction opposite to the flow, with a peak at 4.7 kHz, the vortex shedding frequency.

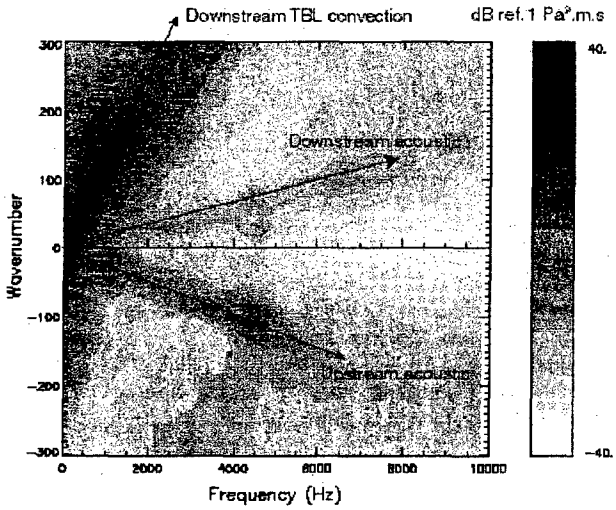

Figure 8 : Same as Figure 7 but x/C = 0.5.

Figure 8 presents the same results obtained at mid chord ($x/C = 0.5$). The convective ridge and the upstream acoustic component are again present. One interesting result is a new component $k = \omega/(a_0 + U_e)$ which corresponds to acoustic waves (also with a peak at 4.7 kHz) propagating in the flow direction (downstream), which may be generated by the diffraction, at the airfoil leading edge, of the acoustic waves propagating upstream.

Flow pressure fluctuations

Instantaneous maps of pressure fluctuations

The existence of a sound field generated at the TE, strongly suggested by the surface pressure results above, is confirmed on Figure 9 which shows instantaneous isovalues of the pressure fluctuations inside the flow. At every point of the LES grid, pressure fluctuations are computed by substracting the time-averaged pressure to the instantaneous pressure. The color table is adapted to the low values of the acoustic fluctuations (± 6 Pa) although there are much larger pressure fluctuations (up to ± 500 Pa) in the TBL and in the wake. Concentric waves are clearly observed near the TE, with a wavelength corresponding to the vortex shedding frequency 4.7 kHz which, as shown before, dominates the source spectrum by a few decibels. An animation was generated from 300 identical maps plotted for successive time steps ($\Delta t = 5.10^{-5}$ s) allowing to simultaneously visualize, with their respective celerity, the acoustic radiation in the fluid and the turbulence convection along the airfoil chord.

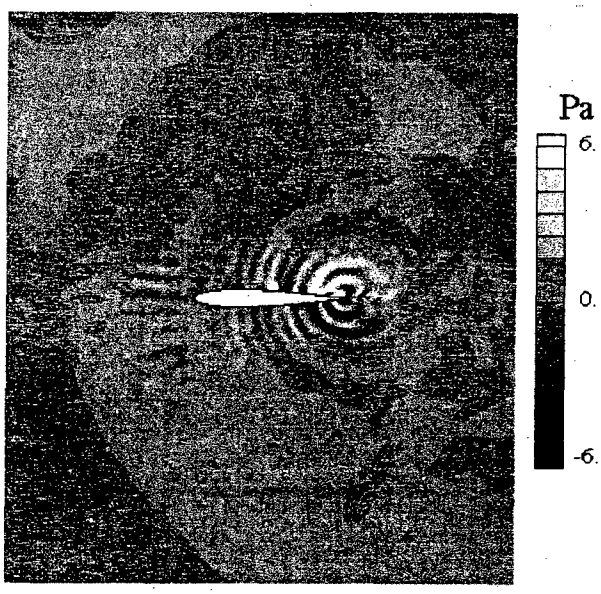

Figure 9 : Instantaneous isovalues of pressure fluctuations obtained from LES data.

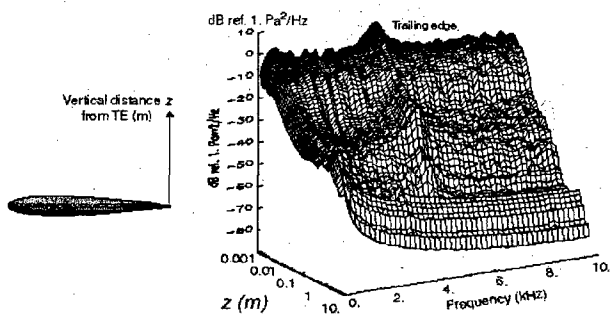

Figure 10 : Evolution of the wall pressure spectra along the vertical grid line x = C (starting from the TE upper corner) with respect to the vertical distance z.

Low-pass filtering by the CFD grid

It is interesting to notice that the wave pattern corresponding to the vortex shedding noise vanishes at a half-chord from the airfoil, when, at the same time, larger wavelength are observed much farther. This is explained by the radial stretching of the grid LES which acts on the noise field as a low-pass filter. It is known that the propagation of an acoustic wave will not be correctly simulated if it is discretized by using less than 4 or 6 cells by wavelength.

To illustrate this, Figure 10 shows the evolution of the wall pressure spectra along the vertical grid line $x = C$ (starting from the TE upper corner) with respect to the distance from the TE (in logarithmic scale). This plot clearly shows that low frequency waves propagate much farther than high frequency waves.

Figure 11 shows the same information for several frequency bandwidths in which spectra are integrated. Each frequency bandwidth shows similar behaviour : (i) at short distance from the TE, spectra are dominated by high-level turbulence ; (ii) then there exists a domain where the pressure fluctuations decrease as $z^{-1/2}$, which is typical of a two-dimensional acoustic field ; (iii) beyond a cut-off distance the levels vanish. It was

checked that, for any frequency bandwidth, this cut-off distance corresponds to a grid location where cells become larger that a quarter acoustic wavelength.

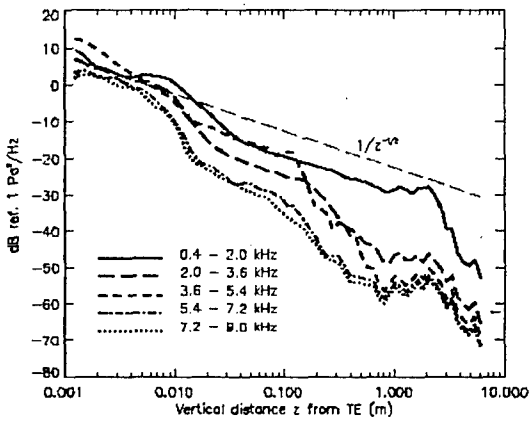

Figure 11 : Same information as in Figure 10, presented in integrated frequency bandwidths

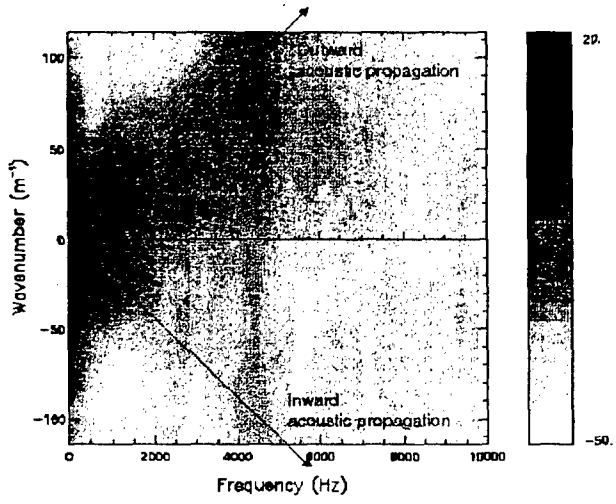

Figure 12 : Same information as in Figures 10 and 11, but presented through a wavenumber-frequency spectrum .

Figure 12 shows a wavenumber frequency spectrum computed from the LES pressure fluctuations field along the same vertical line $x = C$. The ridge located along the "acoustic line" $k = \omega / a_0$ clearly demonstrates the radiative acoustic nature of this pressure field with, again, a peak of power at the vortex shedding frequency 4.7 kHz. A much weaker component is also visible on the line $k = -\omega / a_0$ correponding to waves propagating towards the TE, but this peak lays more than 25 dB below the radiative component and may even not be physical with regards to the resolution of the process.

Spanwise coherences

Inside the TBL and the wake, turbulent structures or eddies are convected at low velocities $(< U_e)$ which means that typical spanwise lengh scales may be smaller than the spanwise extent of the LES domain, and correctly simulated. To illustrate this, Figure 13 shows the spanwise evolution of the coherence $\gamma^2(\Delta y, f)$ of the surface pressure field near the TE in several frequency bandwidths. $\gamma^2(\Delta y, f)$ is defined as :

$$\gamma^2(\Delta y, f) = \frac{|S_{pp}(0, \Delta y, f)|^2}{|S_p(0, f)||S_p(\Delta y, f)|} \qquad (9)$$

where $S_p(y, f)$ denotes the surface pressure spectrum at the spanwise position y and $S_{pp}(y_1, y_2, f)$ denotes the surface pressure cross spectrum between spanwise positions y_1 and y_2. The coherence rapidly vanishes at any frequency bandwidth, meaning that integral length scales are smaller than the spanwise extent of the LES domain. It can be seen that the largest length scales correspond to the vortex shedding frequency, a mechanism which significantly correlated in the spanwise direction. It should be noted that these spanwise coherences provide wall pressure spanwise integral length scales which are favorably compared to experimental values measured by Brooks and Hodgson on their NACA0012 airfoil [24].

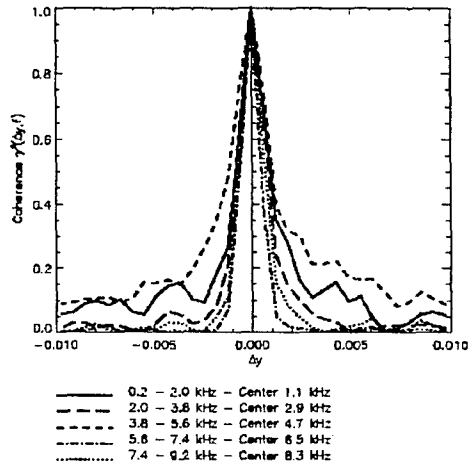

Figure 13 : Spanwise evolution of the coherence of the surface pressure field on the succion side near the TE (x/C = 0.9958). Integrated frequency bandwidths.

Figure 14 shows spanwise coherence of the pressure field above the TE on the grid line $j_n = 54$ located at distance $z_n = 37.9$ mm from the TE, where pressure fluctuations are expected to be mostly acoustic : as explained below, this particular grid line will be chosen for the generation of the integration surface used in the Kirchhoff prediction. Figure 14 shows that typical length scales seem to be much longer than the spanwise extent of the LES grid, especially at low frequency and the frequency of vortex shedding.

In other words, the very nearfield turbulent flow is expected to be strongly three-dimensional, whereas the acoustic field simulated at some distance of the airfoil looks two-dimensional. This result will have significant consequences in the process of spanwise replication of LES data.

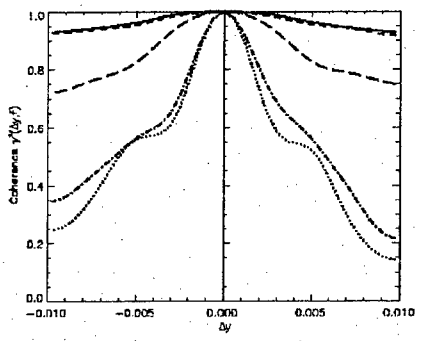

Figure 14 : Spanwise evolution of the coherence of the pressure field above the TE on the grid line $j_0 = 54$ at $x/C = 1$. Same integrated frequency bandwidths as Figure 14.

KIRCHHOFF ACOUSTIC PREDICTION

Introduction

The preceding results show that the compressible LES has the capacity of simulating the generation of the aeroacoustic mechanism of TE noise, including both aerodynamic sources and local radiated field. Unfortunately, due the strong grid stretching, this acoustic field rapidly collapses at rather short distance from the airfoil. As a consequence of the last part, it makes sense to find a surface, enclosing the airfoil, close enough to the body to ensure that the simulated acoustic field has not been low-pass filtered by the grid, or at least still contains the low-frequency bandwidth that we are interested in. Moreover, if this surface can be proved free of any vorticity convected by the flow, it is a perfect candidate for the application of a Kirchhoff integration.

Formulation

A 3D Kirchhoff formulation is implemented in the KIM (Kirchhoff Integration Method) code which was developed at ONERA for helicopter rotor noise prediction [25] and jet noise prediction [26]. This code provides the noise radiated by any three-dimensional surface in a flow with uniform velocity U_0 in the direction X_1, given the density (or pressure, assuming isentropy or $p' = c_0^2 \rho'$) and its normal gradient along this surface.

The formulation is [27] :

$$\rho'\left(\vec{X},t\right) = \iint f_K\left(\vec{X},\vec{Y},\tau\right)\frac{1}{4\pi d}\delta\left(t-\tau+\frac{D_{XY}}{c_0}\right)dSd\tau \qquad (10)$$

in which D_{XY} is the distance, corrected from convection effects, between the source point $\vec{Y}$, located on the integration surface, and the observer point $\vec{X}$ (both defined in a reference framework in which the surface S is at rest) :

$$\begin{cases} D_{XY} = \dfrac{d - M_0\left(X_1 - Y_1\right)}{\beta^2} \\ d = \sqrt{\left(1-\beta^2\right)\delta_{1i} + \beta^2\left(X_i - Y_i\right)^2} \end{cases} \qquad (11)$$

$f_K\left(\vec{X},\vec{Y},\tau\right)$ is given by :

$$f_K\left(\vec{X},\vec{Y},\tau\right) = \frac{\rho'}{d^2}\left(1-M_0^2\right)\vec{n}.\left(\vec{X}-\vec{Y}\right) + M_0^2 n_1 \frac{\partial \rho'}{\partial Y_1} - \frac{\partial \rho'}{\partial n} + \frac{1}{c_0}\left[M_0 n_1 + \frac{\vec{n}.\left(\vec{X}-\vec{Y}\right)}{d}\right]\frac{\partial \rho'}{\partial \tau} \qquad (12)$$

This formulation assumes that the pressure field on S satisfies the convected wave equation :

$$\left(\frac{D^2}{D\tau^2} - a_0^2\Delta\right)\rho' = 0 \text{ with } \frac{D}{D\tau} = \frac{\partial}{\partial \tau} + U_0\frac{\partial}{\partial X_1}, \qquad (13)$$

which governs the propagation of acoustic waves in a medium with uniform velocity U_0 in the direction X_1.

Space-time discretization

The space-time discretization of the Kirchhoff integration on a given closed control surface assumes that temporal fluctuations of fluid pressure are time-sampled (with time step Δt and duration $N\Delta t$) at any cell (with maximal dimension $\Delta\sigma$) of a 2-layer (with maximal normal separation Δn between both layers) surface grid. If λ_a and $T_a = \lambda_a / c_0$ denote the acoustic wavelength and period, the crucial parameters of the process are $\Delta\sigma / \lambda_a$, $\Delta n / \lambda_a$ and $\Delta t / T_a$. These parameters were carefully adjusted on the basis of a parametric study (that can be found in the Annex of Ref. [24]) which was performed before to achieve actual Kirchhoff integration.

Construction of the control surface

Figure 15 shows how the integration surface is constructed from one given C-shaped grid line surrounding the airfoil in domain #1, extended in domain #2 by the two corresponding horizontal grid lines. These horizontal lines are stopped at nearly one third-chord from the TE, where acoustic levels are very low and grid cells become much larger than the acoustic wavelength.

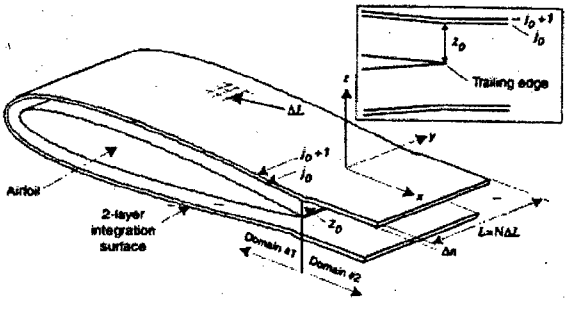

Figure 15 : Kirchhoff integration : construction of the control surface.

Then the three-dimensional surface is obtained by N replications in the spanwise direction along the desired span extent $L = N\Delta L$. In the present application, with reference to Brooks and Hodgson's experiment [24], the airfoil's span was taken equal to $L = 0.46$ m or $0.75C$. N was fixed to $N = 92$ according to a parametric study presented in the Annex of Ref. [24].

It should be noted that the final 3D surface is not closed, neither at its two lateral sides (their contribution to the noise radiated in the z direction is neglectible) nor at its downstream

extremity (which contains very low acoustic levels and may be crossed by undamped vorticity convected in the wake).

The LES 3D grid has a spanwise extent limited to 3.3 % of the airfoil chord, so the LES data have to be extrapolated in the spanwise direction. The 2D behaviour of the simulated acoustic field, especially confirmed by the spanwise coherences presented on Figure 14, suggest to simply replicate, along the whole span L, the 2D field computed at $y = 0$.

Finally the critical design parameter of the integration surface is the index j_0 of the grid line surrounding the airfoil, which varies from $j_0 = 1$ on the airfoil, to $j_0 = 97$ at the grid border. Once this parameter is chosen, the normal separation Δn is directly related to j_0, as grid lines of indexes j_0 and $j_0 + 1$ are used to compute the pressure normal gradients.

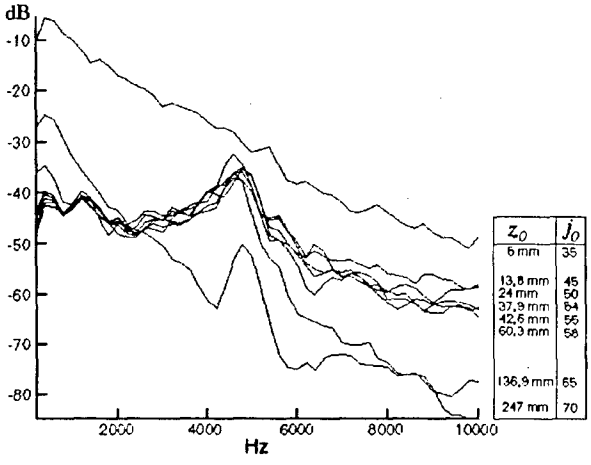

Figure 16 : Parametric study of the position of the Kirchhoff integration surface S (parameters : index j_0 of the used grid line, and normal distance z_0 to the airfoil TE). Noise radiated at $z_0 = 2C$ above the trailing edge.

Figure 16 shows the influence of j_0 on the power spectral density of the noise radiated at $z = 2C$ above the trailing edge, computed by the Kirchhoff integration. It should be noted that all other parameters were adjusted to final values deduced from the parametric studies described in the Annex.

On each presented spectrum, the index j_0 and the distance of the grid line from the airfoil are mentioned. This plot shows that a family of intermediate grid lines provide very similar spectra, which is a good indication of a region where the pressure field is mostly acoustic. The spectra computed from the grid lines nearest to the airfoil are obviously contaminated by intense vorticity convected in the TBL and the wake. On the other hand, spectra computed from farther grid lines are progressively attenuated in the high frequency band, which is another confirmation of the low-pass filtering generated by the grid stretching. The grid line $j_0 = 54$ located at the distance $z_0 = 37.9$ mm from the airfoil was finally chosen for the Kirchhoff computations. The normal distance between lines 54 and 55 is $\Delta n = 4.7$ mm.

Results

Instantaneous pressure distributions

The Kirchhoff integration method offers the conveniency of easily computing the noise at any location outside the control surface. If the available computing resources are sufficient, the noise can be computed at thousands of locations to build instantaneous maps or time-animated pressure distributions.

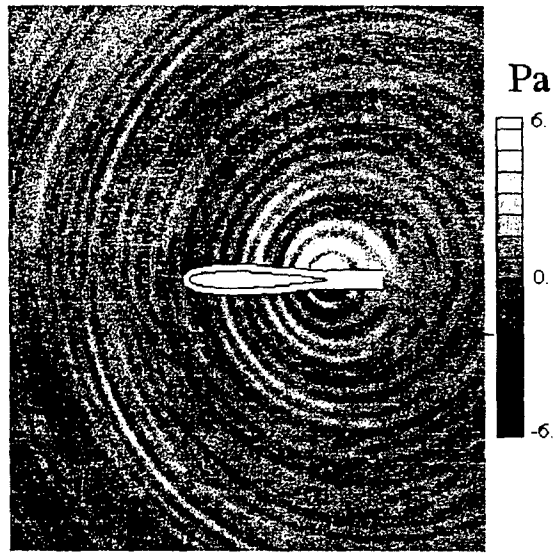

Figure 17 : Noise contours computed via the Kirchhoff method outside the integration surface.

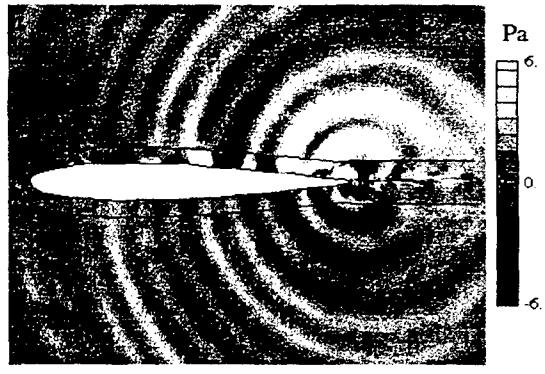

Figure 18: Pressure contours inside (LES) and outside (Kirchhoff) the integration surface

Figure 17 shows such a map computed on a two-dimensional cartesian grid of regular space step $\Delta x = \Delta y = 1.2$ cm which extends two chords around the airfoil. It is interesting to compare this Kirchhoff noise field to the similar result of Figure 9, which was obtained from the LES pressure fluctuation field. Both figures are using the same colour scale, showing how the acoustic field is rapidly filtered and eliminated from the LES data.

Figure 18 provides a closer view of the control surface region, in order to evaluate the continuity between the pressure fields inside and outside the surface. Inside the surface, the pressure field is directly deduced from the LES data as in Figure 9. Outside the surface, the pressure is computed via a Kirchhoff integration as in Figure 17.

Farfield noise

Figure 16 shows noise spectra computed from various Kirchhoff surfaces (including the surface based on the grid line $j_0 = 54$ $z_0 = 37.9$ mm which was finally chosen) at $z = 2C$. This specific position was chosen because it corresponds to the

location of a microphone in the Brooks and Hodgson's experiment [24]. The PSD measured by this microphone is presented on Figure 20 (dashed line). The noise predicted via the Kirchhoff integration overestimates the measured data by more than 15 dB. This overestimation may have several reasons acting together. Firstly, it is important to distinguish the nearfield unsteady CFD and the farfield noise prediction : it has been seen that wall pressure fluctuations already overestimated measured values by 3 to 5 dB, which means that the overprediction by the acoustic prediction may be closer to 10 dB.

Secondly, the spanwise replication of the central pressure field assumes that the acoustic field on the control surface is perfectly correlated (or fully two-dimensional) in the spanwise direction. This assumption was considered in accordance with the spanwise coherences shown on Figure 14. However, it is almost certain that these coherences are artificially overestimated due to the small extent of the LES computational domain (in a similar approach based on the Ffowcs Williams and Hall's TE noise theory applied to incompressible LES, Wang [6] showed that the radiated noise computed from CFD data replicated in the spanwise direction is very sensitive to the spanwise coherence of these data).

FFOWCS WILLIAMS-HAWKINGS INTEGRATION

Formulation

Since wall pressure spanwise coherences (Figure 13) and fluctuation levels (Figure 6) were found to match experimental data, a second noise prediction was achieved using the Ffowcs Williams-Hawkings (FW-H) method (dipole surface term only).

A 3D FW-H formulation is implemented in the FIM (FW-H Integration Method) code which was developed at ONERA for helicopter rotor noise prediction. This code provides the noise radiated by any three-dimensional surface in a flow with uniform velocity U_0 in the direction X_1, given the data ρ, p and ρu_i along this surface. The formulation is[29] :

$$\tilde{p}\left(\vec{X},t\right)=c_0^2\iint f_{FWK}\left(\vec{X},\vec{Y},\tau\right)\frac{1}{4\pi d}\delta\left(t-\tau+\frac{D_{XY}}{c_0}\right)dSd\tau \quad (14)$$

where D_{XY} and d are defined in (11) and :

$$f_{FWK}\left(\vec{X},\vec{Y},\tau\right)=\frac{1}{\beta^2}\frac{\partial}{\partial\tau}\left[\begin{array}{l}\dfrac{1}{c_0^2}\left[\begin{array}{l}\dfrac{\beta^2}{d}\vec{A}.\left(\vec{X}-\vec{Y}\right)+\\ \dfrac{M_0^2}{d}A_1\left(X_1-Y_1\right)-MA_1\end{array}\right]+\\ B\left[1-\dfrac{M_0}{d}\left(X_1-Y_1\right)\right]\end{array}\right]$$
$$+\frac{1}{d^2}\left[\beta^2\vec{A}.\left(\vec{X}-\vec{Y}\right)+\left(M_0^2A_1-U_0B\right)\left(X_1-Y_1\right)\right] \quad (15)$$

and

$$\left\{\begin{array}{l}A_i=\dfrac{1}{c_0^2}\left[\tilde{p}n_i+\rho u_i\left(u_n-v_n\right)\right]\\ B=\dfrac{1}{c_0^2}\left[\rho_0 v_n+\rho\left(u_n-v_n\right)\right]\\ v_n=-U_0n_1\end{array}\right. \quad (16)$$

and all other notations are identical as in the Kirchhoff formulation. It should be noted that this formulation is not complete since it ignores the volume integration term : when the surface is taken at the airfoil wall, the volume outside the surface obviously contains a distribution of quadrupoles, but it is assumed that this term can be neglected (this assumption has been verified in aeroacoustic mechanisms involving solid walls, such as helicopter rotor noise or propeller noise).

Application

The application of the above formulation to the present case relies on the comparison of :

- the spanwise integral length scale of wall pressure fluctuations computed by LES : $\Lambda_y < 3$ mm,
- the spanwise extent of the LES computational domain : $S_{LES} \approx 20$ mm or 3,3 % of the chord,
- the spanwise extent of the real airfoil used in the experiment [24]: $S_{EXP} \approx 0{,}46$ m.

In a first step, the FIM code is used to compute the DSP $\Phi_{LES}(\omega)$ of the noise radiated by a narrow airfoil of span S_{LES}. This is done by using a surface located at the airfoil wall and integrating the data computed via LES on all the 33 planes of the 3D LES domain. It is then assumed that the real airfoil of span S_{EXP} is made of S_{EXP}/S_{LES} narrow airfoils located side-by-side. Since $\Lambda_y < S_{LES}$, any couple of these narrow airfoils behave as fully decorrelated sources and an estimation of the DSP $\Phi_{EXP}(\omega)$ of the noise radiated by the real airfoil of span S_{EXP} is given by :

$$\Phi_{EXP}(\omega)=\frac{S_{EXP}}{S_{LES}}\Phi_{LES}(\omega) \quad (17)$$

Results

Figure 20 shows the noise spectrum estimated via this numerical procedure at $z = 2C$ above the TE. It is compared, without correction or normalisation, to the experimental data obtained by Brooks and Hodgson at the same position.

It is interesting to notice that experiment and simulation differ in the same way (frequency shift and amplitude difference) as wall pressure spectra shown on Figure 6, which may confirm the validity of the acoustic method.

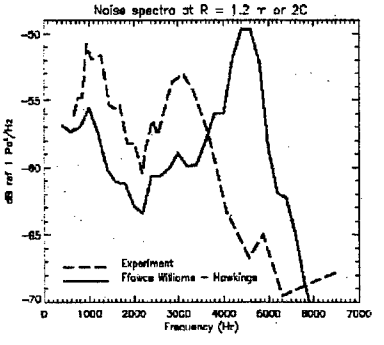

Figure 20 : Power spectral density of the noise radiated at $z = 2C$ above the TE. Comparaison of computed (solid line) and measured (dashed line) data [24].

Directivity diagrams

Figure 21 shows a diagram obtained by computing (with both Kirchhoff and FW-H methods) the noise radiated on equally spaced points located on a circle of radius $r = 1.2$ m (or $2C$) centered on the airfoil TE. The directivity is compared to the theoretical directivity of the noise emitted by turbulence

passing the trailing edge of an infinite half-plane. It is also compared to experimental values given by Brooks and Hodgson [24].

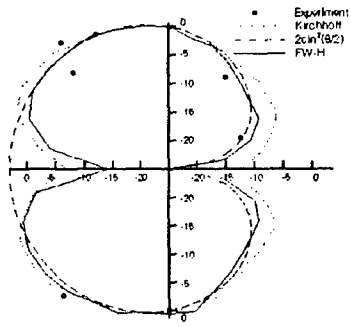

Figure 21 : Directivity diagram of radiated noise on a circle of radius 2C centered on the TE. Comparison of computed data (Kirchhoff and Ffowcs Williams Hawkings methods) with half-plane TE noise and experimental data [24].

LINEARIZED EULER EQUATIONS

The need

Going back to the pressure contours shown on Figure 18 obtained via the Kirchhoff integration, it is interesting to follow the acoustic waves emitted at the TE and propagating in the upstream direction, especially along the pressure side chord on which the TBL is only visible near the TE. At the vicinity of the TE, these waves are rather continuous in both LES and Kirchhoff pressure fields. When they have traveled along more than a half chord, it becomes clear that waves in the LES domain (inside the surface) are slightly slower than their counterpart propagating in the Kirchhoff domain outside the surface. To explain this, one must remember that the Kirchhoff method assumes that the flow outside the controle surface has a uniform velocity U_0, whereas the mean flow simulated via LES inside the control surface present local velocities U_e that may be significantly larger than U_0, especially on the succion side of a lifting airfoil. This last result underlines what is probably the most critical limitation of integral methods such as the Kirchhoff integration : outside a given surface or volume, they do not take into account the inhomogeneities of the mean flow.

This limitation fully justifies the development of a complementary tool based on the discretization of LEE, which have the ability to account for local mean velocity gradients. However, since the application of such methods may become very computationally consuming, especially in complex 3D cases, it should be strictly limited to the regions where strong velocity gradients make it really necessary. In the present problem, such region could be reasonably limited to a domain extending one chord away from the airfoil. Outside this new control surface, the mean flow can be considered as rather uniform and the Kirchhoff method can be applied to provide accurate prediction of the sound at much larger distance from the airfoil.

The E3P code

The E3P code (Propagation via Euler Equations under a Small Perturbation Hypothesis) based on discretized LEE is currently developped at ONERA for this purpose [12]. The formulation is based on the splitting of the total field in a mean flow and a perturbation field. The equations are discretized in conservative form and can be either linearized (only first terms are kept) or not (all linear and non-linear terms are used). Cartesian or curvilinear 2D/3D (monodomain) structured grids can be used. In the space domain, the discretization uses high order finite differente explicit or implicit schemes. In the time domain, multi-steps schemes (Adams-Bashford or Runge-Kutta) are used. Specific boundary conditions are implemented for solid surfaces, non-reflexive border, periodicity or data injection. Non-uniform mean flows are taken into account. The next part shows several configurations of acoustic scattering problems solved with this code. The last paragraph explains how this code could be coupled with unsteady CFD computations.

Acoustic scattering using E3P

Figure 22 shows the free-field radiation of an acoustic harmonic Gaussian source in a steady uniform flow at Mach 0.5, computed on a 200×200 weavy grid and compared with the analytic solution.

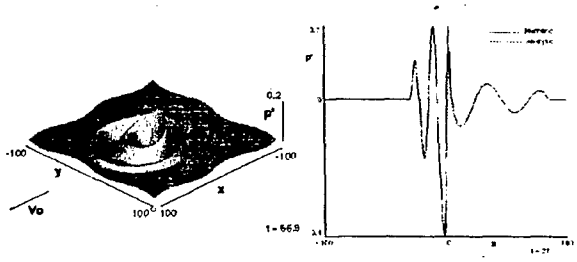

Figure 22 :Radiation of a harmonic Gaussian source in a uniform flow $M = 0.5$. E3P, weavy grid 200×200, compared with analytic solution.

Figure 23 shows the acoustic scattering of a harmonic source on a rigid circular cylinder of radius a in a fluid at rest. The RMS pressure field (amplitude and phase) along a circle of radius $2a$ is compared with results obtained with a Boundary Element Method (BEM). Figure 24 shows the same configuration, but with a non uniform (potential) mean flow around the cylinder. Figure 25 shows the acoustic scattering of a harmonic source on a rigid elliptic cylinder.

Figure 26 shows the acoustic scattering of a harmonic source on a rigid Joukowski airfoil in a potential mean flow. Figure 27 displays three-dimensional computation of the acoustic scattering of a harmonic source on a 3D rigid circular cylinder, again and with a potential mean flow.

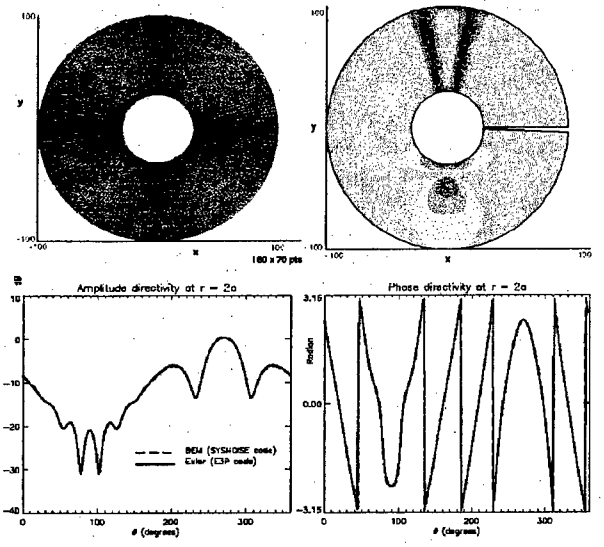

Figure 23 : Acoustic scattering of an harmonic source on a rigid circular cylinder (M = 0) of radius a. Cylindrical grid. RMS pressure field. Comparison of RMS pressure (amplitude and phase) at radius 2a with Boundary Element Method (BEM).

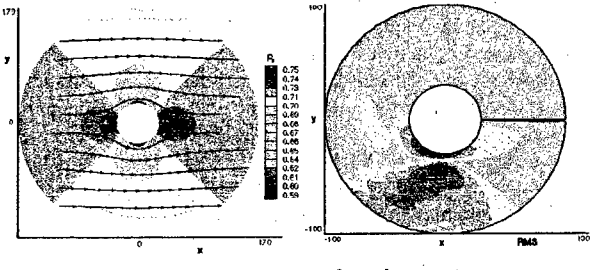

Figure 24 : Acoustic scattering of an harmonic source on a rigid circular cylinder with potential non-uniform mean flow (M = 0.3). RMS pressure field.

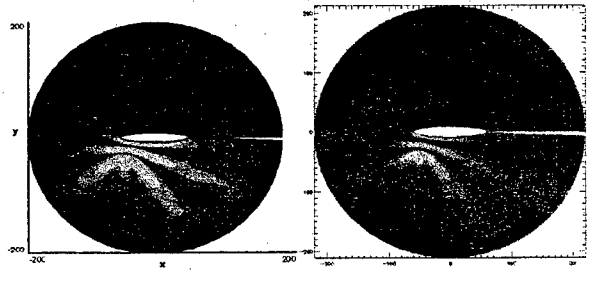

Figure 25 : Acoustic scattering of an harmonic source on a rigid elliptic cylinder (M = 0). Comparison of amplitude RMS pressure field (LHS)) with BEM results (RHS).

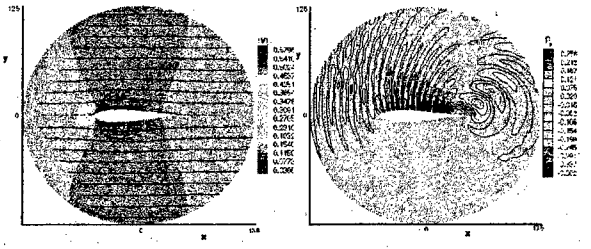

Figure 26 : Acoustic scattering of an harmonic source on a rigid Joukowski airfoil with potential non-uniform mean flow (M = 0.3). RMS pressure field.

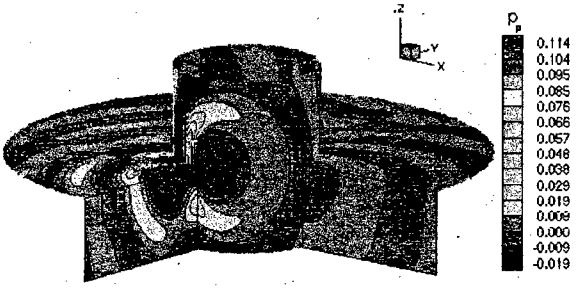

Figure 27 : Acoustic scattering of an harmonic source on a rigid 3D circular cylinder with potential non-uniform mean flow (M = 0.3). RMS pressure field.

Toward coupling LEE with LES

The coupling of local unsteady CFD with discretized LEE is a complex problem. Up to now, most applications were based on the formulation of volume distribution of aeroacoustic sources constructed from the CFD results and used as right-hand-side source terms in Euler equations.

In the present application, it was shown that compressible LES is able to simulate the generation and local propagation of noise. This result suggests that LES could be coupled with the noise E3P code using a surface interface similar to the Kirchhoff control surface. This basic principle requires that a perturbation field can be injected at one border of a LEE domain, a functionality which, in a first step, was tested by injecting an acoustic field radiated by an harmonic source located outside the LEE domain.

Figure 28 shows such validation in the case of a a cylindrical grid. The (virtual) monopole is located inside the inner border of the domain, and its (analytical) field is injected on this inner border. The acoustic field computed in the LEE domain is favorably compared with the analytical field.

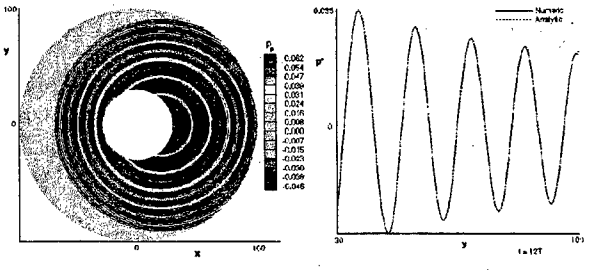

Figure 28 : Injection, at the inner border of a cylindrical grid, of the acoustic field radiated by a (virtual) monopole located inside the inner border. Comparison with the analytical field.

On Figure 29 the same analytical acoustic field is injected at the inner border of a grid which was derived from the LES grid shown on Figure 1. Again, the pressure field computed in the LEE domain is favourably compared with the abanlytical direct propagation. The next step will consist in injecting LES data at the same inner border.

It is believed that the next significant results of CAA applied to airfoil noise predictions will be obtained via the combination of (i) unsteady CFD (LES) for the nearfield flow, (ii) the linearized Euler equations for intermediate acoustic sound field and (iii) an integral method (Kirchhoff, Ffowcs Williams-Hawkings) for the prediction of the far field noise.

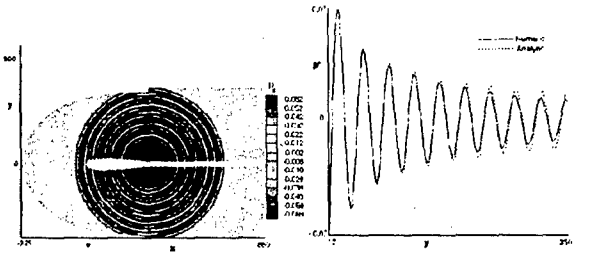

Figure 29 :Injection, at the inner border of a CFD grid, of the acoustic field radiated by a (virtual) monopole located inside this inner border. Comparison with the analytical field.

CONCLUSIONS

The unsteady flow past an isolated NACA0012 airfoil with a constant section and a blunted TE is computed via compressible LES. Detailed analysis of the results shows that the unsteady flow is accompanied by an acoustic field generated by the acoustic scattering of (i) the turbulent boundary layers convected on both airfoil sides (broadband noise) and (ii) the alternated vortex shedding generated by the TE bluntness (narrow band component). A close examination of surface pressure fluctuations near the TE shows that spanwise integral length scales are probably smaller than the computational domain extent in that direction, although the latter only represents 3.3 % of the chord. Surface pressure spectra are compared with published experimental data obtained on the same airfoil geometry. The computed vortex shedding frequency is slightly higher than the measured one, which can be explained by an underestimation of the TBL thicknesses. Predicted levels also slightly overestimate measured levels. Due to the strong stretching of the LES computational grid, which acts as an acoustic low-pass frequency filter, this acoustic field cannot radiate farther than a half-chord from the body.

In a second step, the LES has been relayed by an acoustic propagation method to simulate the farfield noise. For this purpose, two different integral methods have been used, a Kirchhoff integration and a Ffowcs Williams-Hawkings integration.

The Kirchhoff control surface is constructed via the spanwise development of a grid line surrounding the airfoil. This method necessitates a careful study of several critical parameters such as the position of the control integration surface enclosing the airfoil and its wake, the spanwise replication step, the distance between the two layers of the surface (for correct computation of pressure normal gradients) and the time step, all parameters being normalized by the acoustic wave length or time period. Since the acoustic field generated at the TE shows strong two-dimensional characteristics, the pressure field on the integration surface is simply obtained by replicating the LES data in the spanwise direction. Predicted farfield noise spectra are compared with published experimental data obtained in an anechoic facility with the same airfoil geometry (but much larger span). Predicted levels overestimate experimental spectra, which is most probably due to the assumption that the acoustic field is fully correlated along the spanwise extent of the integration surface, which is obviously only true at very low frequencies and in the frequency domain of the vortex shedding.

In a second step, the Ffowcs Williams-Hawkings method was used along with wall pressure data which provided spanwise correlations matching experimental values. In this case, the far field noise spectrum is obtained in two steps. In a first step, the noise radiated by an narrow airfoil is obtained by integrating wall pressure data in the whole LES computation domain. Then the noise radiated by an airfoil with realistic span is obtained by summing decorrelated contributions of several identical narrow airfoils lying side-by-side. Final results favorably agree with experimental measurement.

Finally, close examination of acoustic waves propagating (i) in the LES pressure field inside the controle surface and (ii) in the Kirchhoff pressure field outside the surface, clearly shows the influence of the uniform-flow assumption which is implicit in most integral methods. This strongly justifies the use of a novel acoustic method based on the discretized LEE. This method is currently under development. Several solutions of acoustic scattering problems were solved with this code and are presented. Then it is shown how this tool could be combined with nearfield LES on the basis of a 2D interface. It is believed that this combination will soon bring significant progress in the field of the numerical prediction of airframe noise.

ACKNOWLEDGEMENTS

This work was funded by the SPAé (Office of Aeronautical Programs). The results presented in this paper were partly communicated at the 7th AIAA/CEAS Aeroacoustic Conference in Maastricht (NL) in May 2001 [12, 28] and at the 17th International Congress on Acoustics in Roma (IT) in September 2001 [30].

The authors are grateful to Gilles Rahier at ONERA for his valuable contribution to the adaptation of the KIM (Kirchhoff Integration Method) and FIM (Ffowcs Williams-Hawkings Integration Method) codes to the present application.

BIBLIOGRAPHY

1. Kalizin N. and Kalitzin G. *"Influence of Turbulent Models on SNGR Sound Predictions of Flow over Trailing Edge of a Flat Plate"*, AIAA Paper No. 2000-1982, 6th AIAA-CEAS Aeroacoustics Conference, Lahaina (Hawaii), 12-14 June, 2000.
2. Singer B.A., Brentner K.S., Lockard D.P. and Lilley G.M. *"Simulation of Acoustic Scattering from a Trailing Edge"*, AIAA Paper 99-0231, 37th Aerospace Sciences Meeting and Exhibit, Reno (NV), Jan. 12-15, 1999.
3. Singer B.A., Lockard D.P., Brentner K.S. *"Computational Aeroacoustic Analysis of Slat Trailing-Edge Flow"*, AIAA Journal, Vol. 38, No. 9, pp. 1558-1564, September, 2000.

4. Spyropoulos E.T. and Holmes B.S. *"Computation of the airframe noise of a wing-flap configuration"*, AIAA Paper 99-1801, 5th CEAS/AIAA Aeroacoustics Conference, Seattle, USA, 10-12 May, 1999.
5. Manoha E., Troff B. and Sagaut P. *"Trailing Edge Noise Prediction using Large Eddy Simulation and Acoustic Analogy"*, AIAA Journal, Vol. 38, No. 4, pp. 575-583, April (also AIAA Paper 98-1066), 2000.
6. Wang M. and Moin P. *"Computation of Trailing-Edge Flow and Noise Using Large-Eddy Simulation"*, AIAA Journal, Vol. 38, No. 12, pp. 2201-2209, December, 2000.
7. Lighthill M.J. *"On sound generated aerodynamically. I. General theory II. Turbulence as a source of sound"*, Proc. Roy. Soc. Lond., Vol. A 211, pp. 564-587, 1952. Vol. A 222, pp. 1-32, 1952.
8. Ffowcs Williams J.E. and Hawkings D.L. *"Sound generation by turbulence and surfaces in arbitrary motion"*, Phil. Trans. Royal Soc., Vol. A 264, pp. 321-342, 1969.
9. Manoha E., Elias G., Troff B. and Sagaut P. *"Towards the Use of Boundary Element Method in Computational Aeroacoustics"*, AIAA Paper 99-1980, 5th CEAS/AIAA Aeroacoustics Conference, Seattle, USA, 10-12 May, 1999.
10. Tam C.K.W. and Webb, J.C. *"Dispersion-Relation-Preserving Finite Difference Schemes for Computational Acoustics"*, Journal of Computational Physics, Vol. 107, pp. 262-281, 1993.
11. Grogger H.A., Delfs J.W., Lauke T.G., Lummer M. and Yin J. *"Simulation of leading-edge noise of airfoils using CAA based on body-fitted grids"*, 7th International Congress on Sound and Vibration, Garmisch-Partenkirchen, Germany, 4-7 July, 2000.
12. Redonnet S., Manoha, E. and Sagaut P. *"Numerical Simulation of Propagation of Small Perturbations interacting with Flows and Solid Bodies"*, AIAA Paper n° 2001-2223, 7th CEAS/AIAA Aeroacoustics Conference, Maastricht, The Netherlands, 28-30 May, 2001.
13. Ffowcs Williams J.E. and Hall L.H. *"Aerodynamic sound generation by turbulent flow in the vicinity of a scattering half plane"*, Journal of Fluid Mechanics, Vol. 40, pp. 657-670, 1970.
14. Péchier M. *"Prévisions numériques de l'effet Magnus pour des configurations de munitions"*, Thèse de l'Université de Poitiers, 1999.
15. Péchier M., Guillen P. and gayzac R. *"Magnus Effect over Finned Projectiles"*, J. of Aircraft and Rockets, 2001.
16. Sagaut P. *"Large Eddy Simulatiosn of incompressible flows. An introduction"*, Springer-Verlag, 2001.
17. Lenormand E., Sagaut P. and Ta Phuoc L. *"Large Eddy Simulations of Subsonic and Supersonic Channel Flow at Moderate Reynolds Number"*, Int. J. Numer. Meth. Fluids, Vol. 32, pp. 369-406, 2000.
18. Lenormand E., Sagaut P., Ta Phuoc L. and Comte P. *"Subgrid-Scale Models for Large Eddy Simulations of Compressible Wall Bounded Flows"*, AIAA Journal, Vol. 38, pp. 1340-1350, 2000.
19. David E. *"Modélisation des écoulements compressibles et hypersoniques : une approche instationnaire"*, Thèse de l'Institut National Polytechnique de Grenoble, 1999.
20. Yoon S. and Jameson A. *"An LU-SSOR Scheme for the Euler and navier-Stokes Equation"*, AIAA-Paper n° 87-600, 1987.
21. Mary I. and Sagaut P. *"Large Eddy Simulation of Flow around a high lift airfoil"*, AIAA Paper 2001-2559, 15th CFD Conference, Anaheim (Ca), 11-14 June, 2001.
22. Weber C. and Ducros, F. *"Large-Eddy and Reynolds-Averaged Navier-Stokes Simulation of Turbulent Flow over an airfoil"*, Int. J. CFD, Vol. 13, pp. 327-355, 2000.
23. Wu X., Jacobs R., Hunt J. and Durbin P. *"Simulation of Boundary layer Transition Induced by Periodically Passing Wake"*, J. Fluid Mech., Vol. 398, pp. 109-153,, 1999.
24. Brooks T.F. and Hodgson T.H. *"Prediction and comparison of trailing edge noise using measured surface pressures"*, Journal of Sound and Vibration, Vol. 78 (1), pp. 69-117, 1981.
25. Rahier G., Prieur, J. *"An Efficient Kirchhoff Integration Method for Rotor Noise Prediction Starting Indifferently from Subsonically or Supersonically Rotating Meshes"*, 53rd Annual Forum of the American Helicopter Society, Virginia Beach, VA, April-May, 1997.
26. Seror C., Sagaut P., Rahier G. *"Prévision du bruit de jet de l'ATSF : simulation aéroacoustique d'un jet supersonique à section rectangulaire"*, RTS ONERA n° 12/4418 DSNA/Y, Février 2000.
27. Prieur J. and Rahier, G.,. *"Comparison of Ffowcs Williams-Hawkings and Kirchhoff Rotor Noise Calculations"*, 4th AIAA/CEAS Joint Aeroacoustics Conference, Toulouse, Juin, 1998.
28. Manoha E., Delahay C., Ben Khelil S., Guillen P., Sagaut P. and Mary Y.*"Numerical prediction of the unsteady flow and radiated noise from a 3D lifting airfoil"*, AIAA Paper 2001-2133, 7th CEAS/AIAA Aeroacoustics Conference, Maastricht, The Netherlands, 28-30 May, 2001.
29. Ffowcs Williams J.E. and Hawkings D.L. *"Sound generation by turbulence and surfaces in arbitrary motion"* Phil. Trans. Royal Soc., Vol. A 264, pp. 321-342, 1969.
30. Manoha E., Delahay C., Redonnet S., Sagaut P., Mary I., Ben Khelil S. and Guillen P., *"The Numerical Prediction of Airfoil Trailing Edge Noise"*, 17th International Congress on Acoustics, Roma (IT), 3-7 September, 2001